Large-Scale Simulation of Adhesion Dynamics for End-Grafted Polymers

Scott W. Sides,* Gary S. Grest, and Mark J. Stevens

Sandia National Laboratories,† Albuquerque, New Mexico 87185-1411

Received August 16, 2001; Revised Manuscript Received October 19, 2001

ABSTRACT: The adhesion between a polymer melt and substrate is studied in the presence of chemically attached chains on the substrate surface. Extensive molecular dynamics simulations have been carried out to study the effect of temperature, tethered chain areal density (Σ), tethered chain length (N_t), chain bending energy (k_θ), and tensile pull velocity (v) on the adhesive failure mechanisms of pullout and/or scission of the tethered chains. We observe a crossover from pure chain pullout to chain scission as N_t is increased. Below the glass transition, the value of N_t for which this crossover begins approaches the bulk entanglement length N_e. For the values of N_t and Σ used here, no crossover to crazing is observed.

I. Introduction

Adhesion at polymer interfaces is important in many diverse applications such as colloidal stabilization,[1,2] filler modification of polymeric materials and lubrication,[3] and enhancing mechanical properties of polymer blends.[4,5] The interface of interest can be either (i) between two homopolymer melts (A + B) or (ii) between a homopolymer melt and a hard surface (A + substrate). Most polymer blends do not mix, because even a weak repulsive interaction causes the system to phase separate as the chain length increases. This phase separation reduces entanglements at the interface, and the adhesive strength is then due to relatively weak van der Waals forces alone. For case ii, the interfacial strength depends on the number of chemical bonds between monomers of the polymer and sites on the substrate. In the absence of strong chemical bonding, the adhesive strength is again dominated by weak van der Waals attractions. For both cases certain additives or compatibilizers can increase the adhesive strength of the interfaces. For case i, the additive can be an AB diblock copolymer. The A(B) block of the copolymer can form entanglements with the A(B) melt side. In case ii, the additive is a chain of the A species with a functionalized end group able to react with the substrate, thereby forming a strong chemical bond. The tethered chain of the A species can then become entangled with the melt. In both cases, larger numbers of polymer entanglements result in increased interfacial strength. The systems simulated in this paper consist of substrate-tethered chains in contact with a polymer melt (i.e., case ii), but the results can easily be generalized to polymer/polymer interfaces.

Two key parameters govern the amount of interfacial entanglement, the length (N_t), and the areal density (Σ) of the tethered chains. Adhesion enhancement due to a tethered polymer layer shows a surprising nonmonotonic behavior as a function of N_t and Σ due to the phase behavior for the tethered chain layer.[6−9] The increased work of adhesion W^* for an elastomeric system vs areal density of grafted chains Σ is shown schematically in Figure 1. W^* is defined as the extra work needed to separate two surfaces in addition to the work exerted against dispersion forces alone. In region I where each tethered chain is isolated from its neighbors, the work of adhesion increases as Σ increases. However, as Σ continues to increase, the tethered chains begin to overlap and phase separate from the melt (region II). In this regime, the interpenetration of the tethered chains into the polymer melt decreases with increasing Σ, and as a result W^* decreases. At sufficiently high areal densities, the polymer melt is completely expelled from the tethered chains, thereby causing the work of adhesion to fall off to the bare value due to dispersion forces only (region III). W^* has a similar dependence on N_t. This nonmonotonic behavior has been observed by Léger and co-workers[9,10] in elastomeric materials. Kramer and co-workers[11−15] have studied the effects of tethered chains in glassy polymer systems where the effects of crazing could complicate the dependence of W^* on Σ. While Figure 1 relates the macroscopic work of adhesion to tethered-chain parameters, it does not address the *microscopic* processes involved in adhesion failure at the melt/tethered-chain interface. This paper investigates the effects of N_t, Σ, T, k_θ, and v on these failure mechanisms.

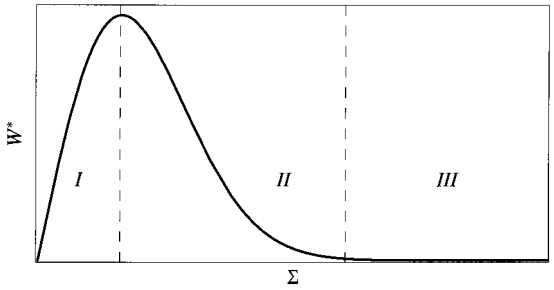

Figure 1. Schematic of the increased work of adhesion W^* for an elastomeric system vs areal density of tethered chains Σ: (region I) mushroom regime; (region II) partially overlapped (wet brush) regime; (region III) phase-separated regime. W^* shows a similar dependence on N_t.

The interplay between the microscopic failure mechanisms of tethered chain pullout and scission (including their possible relationship to crazing) is not fully understood, partly due to the difficulty of direct experimental observation of these phenomena. Molecular

† Sandia is a multiprogram laboratory operated by Sandia Corporation, a Lockheed Martin Company, for the United States Department of Energy under Contract DE-AC04-94AL85000.

10.1021/ma0114739 CCC: $22.00
Published on Web 12/11/2001

dynamics (MD) simulations of fracture in highly cross-linked systems[16,17] and crazing[18,19] have helped to elucidate the crossover from adhesive to cohesive failure of polymer adhesives near walls *without* end-tethered chains. Simulations of tethered chains on small, highly simplified models in 2D have been performed[20,21] but did not study the effects of chain scission in particular. This paper extends the results on our earlier work[22] of large-scale simulations to study the adhesive failure mechanisms of end-tethered chains in contact with an entangled polymer melt. Section II contains details related to the MD simulations and the method used to implement breakable bonds. In section III results of the MD simulations are presented, and conclusions are given in section IV.

II. MD Model/Method

We perform continuous-space, molecular dynamics (MD) simulations on a coarse-grained model of polymer chains. The polymers are represented by attaching N_t spherical beads of mass m with breakable springs. Bead trajectories are obtained by stepwise integration of Newton's equations of motion (EOM) using a velocity Verlet[23] algorithm with a time step $\Delta t = 0.006\tau$, where $\tau = \sigma(m/\epsilon)^{1/2}$, with σ and ϵ setting the length and energy scales, respectively. The EOM includes terms for a weak stochastic force and a viscous drag force with a coefficient on the viscous force term of $0.5\tau^{-1}$.[24] The addition of these two forces to the EOM effectively couples the system to a heat bath. Each pair of monomers separated by a distance r interacts through a standard (12−6) Lennard-Jones potential $U_{LJ}(r)$,

$$U_{LJ}(r) = \begin{cases} 4\epsilon\left[\left(\frac{\sigma}{r}\right)^{12} - \left(\frac{\sigma}{r}\right)^{6}\right] & r < r_c \\ 0 & r > r_c \end{cases} \quad (1)$$

with $r_c = 2.2\sigma$. For simplicity, the substrate interaction is modeled as a flat wall by an integrated LJ potential

$$U_{LJ}^{wall}(z) = \begin{cases} \frac{2\pi\epsilon_{wall}}{3}\left[\frac{2}{15}\left(\frac{\sigma}{z}\right)^{9} - \left(\frac{\sigma}{z}\right)^{3}\right] & z < z_c^{wall} \\ 0 & z > z_c^{wall} \end{cases} \quad (2)$$

with $z_c^{wall} = 2.2\sigma$, $\epsilon_{wall} = 2.0\epsilon$ (strongly attractive wall, no tethered chains), and $\epsilon_{wall} = 0.1\epsilon$ (weakly attractive wall, tethered chains).

To study the effect of chain scission on adhesion, the standard finite extensible nonlinear elastic (FENE) potential[24] is altered to allow for broken bonds along a polymer chain. The total nonbreakable potential $U_{nb}(r)$ (including the FENE potential) between two adjacent beads on the same chain separated by a distance r takes the form

$$U_{nb}(r) = \begin{cases} U_{LJ}(r) + -0.5kR_0^2 \ln\left[1 - \left(\frac{r}{R_0}\right)^2\right] & r < R_0 \\ \infty & r > R_0 \end{cases} \quad (3)$$

while the breakable potential, $U_b(r)$, takes the form

$$U_b(r) = \begin{cases} U_{LJ}(r) + k'r^4[(r - r_1)(r - r_2)] + U_c & r < r_{br} \\ 0 & r > r_{br} \end{cases} \quad (4)$$

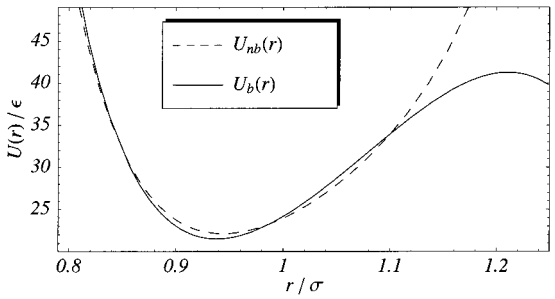

Figure 2. Comparison of the breaking potential $U_b(r)$ and the unbreakable FENE potential $U_b(r)$.

with r_{br} the length at which a chain bond is defined as broken. MD simulations on a similar coarse-grained model[24] using the FENE potential provide details of the chain conformations needed to construct the appropriate starting states. The parameters in the bond-breaking potential come from fitting $U_b(r)$ to the region of the aforementioned FENE potential ($k = 30.0\epsilon/\sigma^2$ and $R_0 = 1.25\sigma$) near its mean equilibrium bond length. This fitting procedure results in $r_{br} = 1.21\sigma$ and a bond-breaking barrier $\Delta U_b \approx 20\epsilon$. The remaining parameters in $U_b(r)$ are $k' = -409.12\epsilon/\sigma^6$, $r_1 = 1.2\sigma$, $r_2 = 1.219\sigma$, and $U_c = 42.059\epsilon$. Fitting $U_b(r)$ to a FENE potential this way allows constructing an initial configuration with chains of approximately the correct radius of gyration R_g by utilizing the aforementioned chain-building algorithm.[24] Figure 2 compares the standard nonbreakable potential to the breakable potential used in this study. The form of $U_b(r)$ allows for two extrema in the bond potential: one stable, global minimum near the FENE potential energy minimum and one local maximum near r_{br} where the bond force becomes zero. This allows bonds to be removed safely from the force calculation without causing large recoil velocities on the resulting chain ends.

The model outlined above results in completely flexible chains. Experimentally, real polymer chains are not completely flexible but have some degree of stiffness. Chain stiffness is added to the model by adding a bending potential energy for each triplet of consecutive particles along a chain. The bending potential takes the form[25]

$$U_\theta(\theta) = k_\theta(1 + \cos\theta)$$

with an equilibrium angle of $\theta_0 = \pi$ where θ is defined in Figure 3. When a bond between two monomers is broken during a simulation, all of the triplets associated with that bond are removed from the force calculation.

The initial chain configurations must be constructed appropriately for the model and potential parameters chosen. For the systems of very long, entangled chains used in this study, it is not feasible to equilibrate the chains by brute-force MD simulation. In general, it is not known how to construct the correct configurations for end-tethered chains next to a long-chain melt. To avoid difficulties in initializing systems for the various wet brush regimes, we restrict the present study to areal densities Σ in the so-called "mushroom regime"[6,7] (i.e., region I in Figure 1). In this regime each tethered chain interacts weakly with other tethered chains and may be constructed as a Gaussian chain. So, for a given N_t and Σ, all chains are constructed as random walks with the correct mean value of R_g. The tethered chains are attached to the substrate wall in random locations. The

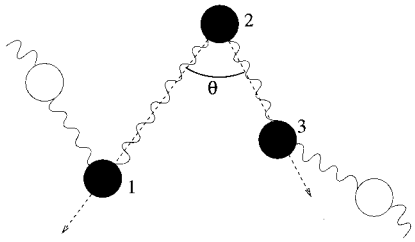

Figure 3. Schematic for bending potential. The three labeled monomers define the triplet used in calculating the bending force associated with the angle θ.

correct value of R_g depends on k_θ, which is known from recent bulk simulations.[26] The system size is adjusted so that the tethered chains do not bridge the box, thereby interacting with the opposite wall. A soft potential is used initially to remove overlaps prior to switching on the full LJ potential between monomers. The size of the simulation cell is adjusted until the pressure $P \approx 0$, resulting in an overall monomer density of $\rho \approx 0.85\sigma^{-3}$($\rho \approx 0.88\sigma^{-3}$) for the highest (lowest) temperatures used. For all simulations, the number of beads in each of the melt chains is $N_m = 2500$ and the number of tethered chains is $n_t = 30$. The chain stiffness is taken to be either $k_\theta = 0$ (fully flexible) or $k_\theta = 1.5\epsilon$ for which the entanglement length as calculated from the plateau modulus is $N_e = 72$ and 27 monomer units, respectively.[27,28] The temperatures used range from $T = 1.0\epsilon/k_B$, which is well above the glass transition temperature for fully flexible chains $T_g = 0.5-0.6\epsilon/k_B$,[18] down to $T = 0.3\epsilon/k_B$. Areal densities as low as $\Sigma = 0.002\sigma^{-2}$ with $T = 1.0\epsilon/k_B$ and $v = 0.0167\sigma\tau^{-1}$ were used without any significant differences with runs using the same parameters for $\Sigma = 0.008\sigma^{-2}$. These results confirm the estimates of Σ which place a system in the mushroom regime. Therefore, to increase computational speed, the majority of the simulations (all the data presented in this paper) use $\Sigma = 0.008\sigma^{-2}$. For systems with cross-linking, the potential for the cross-links is the same as the interactions between monomers bonded along a chain. The cross-links are randomly distributed in the system at an average distance along each chain of approximately 70 monomers, which is comparable to N_e for the fully flexible case. The cross-links are added only to the melt chains after the chain configurations have been constructed and equilibrated. Simulation are performed using the massively parallel MD code LAMMPS[29] (suitably adapted to include chain scission) developed at Sandia and run on the ASCI Red Teraflop machine and Computational Plant (Cplant) clusters.

Figure 4 shows chain configurations at different times from a tensile pull simulation consisting of approximately 7×10^4 particles with $N_t = 100$. Figure 5 shows chain configurations at different times from a tensile pull simulation consisting of approximately 2×10^5 particles with $N_t = 250$. Our largest systems contain close to 10^6 particles. The tensile pull is achieved by moving only the bottom wall at constant velocity. The tethered chains are bonded to the bottom wall of the simulation cell, and the top wall has no tethered chains. The interaction strength of the top wall is set to be sufficiently strong so that no adhesive failure occurs on the top wall during pulling. The interaction of the bottom wall with the melt has a very weak attractive component, so that the adhesion enhancement due to the tethered chains may be studied independently of the adhesion to the bare wall. The z axis is normal to both walls and periodic boundary conditions are used in the x and y directions. The size of the simulation cell in the z direction is set to be approximately 3 times the radius of gyration of the tethered chains prior to pulling. The red chains are tethered, blue chains represent the melt, and green chains were initially tethered and have broken sometime during the tensile pull. Figures 4 and 5 show the qualitative dependence of the tethered chain dynamics on N_t. For small N_t, almost all of the tethered chains are completely pulled out of the melt. For relatively large N_t, all of the tethered chains break somewhere along their length before being totally extracted from the melt.

III. Results

During the simulation we measure the total work exerted and the number of bonds broken by pulling the bottom wall. If $w(t)$ is the instantaneous work at time t, then the total integrated work at t is

$$\mathscr{W}(t) = \int_0^t w(t')\, dt'$$

To quantify the degree of scission, the remaining length of the tethered chains is averaged at the end of a pull simulation. The average fractional length of the remaining chains is

$$\langle F \rangle = \frac{1}{n_t}\sum_i^{n_t} \frac{N_{t,i}^f}{N_t}$$

where $N_{t,i}^f$ is defined to be length of the ith tethered chain at the end of a pull simulation and n_t is the number of chains tethered to the pulling wall. The value of $\langle F \rangle$ quantifies the amount of scission in the tethered chains at the end of a pull. $\langle F \rangle = 1$ corresponds to pure chain pullout and $\langle F \rangle = 0$ to chain scission at the wall for each chain.

A. Chain Length Dependence. Figure 6 shows the integrated work over time as a function of time, $\mathscr{W}(t)$, at different values of N_t for $T = 0.3\epsilon/k_B$, which is well below T_g. For each tethered chain length, $\mathscr{W}(t)$ is measured for a sufficiently long time such that each of the tethered chains have either completely pulled out or broken. The plateau in $\mathscr{W}(t)$ at large t signifies the complete debonding of the pulling surface from the entangled melt. Surfaces with longer tethered chains require more work to completely pull away from the polymer melt than do short chains. However, the maximum work required for surface debonding saturates for large N_t. This effect can be explained by examining the chain length dependence on tethered chain scission.

Figure 7a shows $\langle F \rangle$ vs N_t for two values of v at a temperature well above the glass transition. For $N_t \lesssim 50$ the chains completely pull out of the melt with no breaking. For $N_t \gtrsim 50$ only a fraction of each tethered chain pulls out of the melt before breaking. For the longer tethered chain lengths the value of $\langle F \rangle$ first decreases and then saturates, consistent with the data for $\mathscr{W}(t)$ shown in Figure 6. These data show the entanglement length of the tethered chains to be an important length scale. For the fully flexible model ($k_\theta = 0.0$), $N_e \cong 72$, which is consistent with a value between 50 and 100 for the location of the crossover to chain scission for the faster pulling velocity in Figure 7a. Figure 7b shows $\langle F \rangle$ vs N_t for two values of v for T

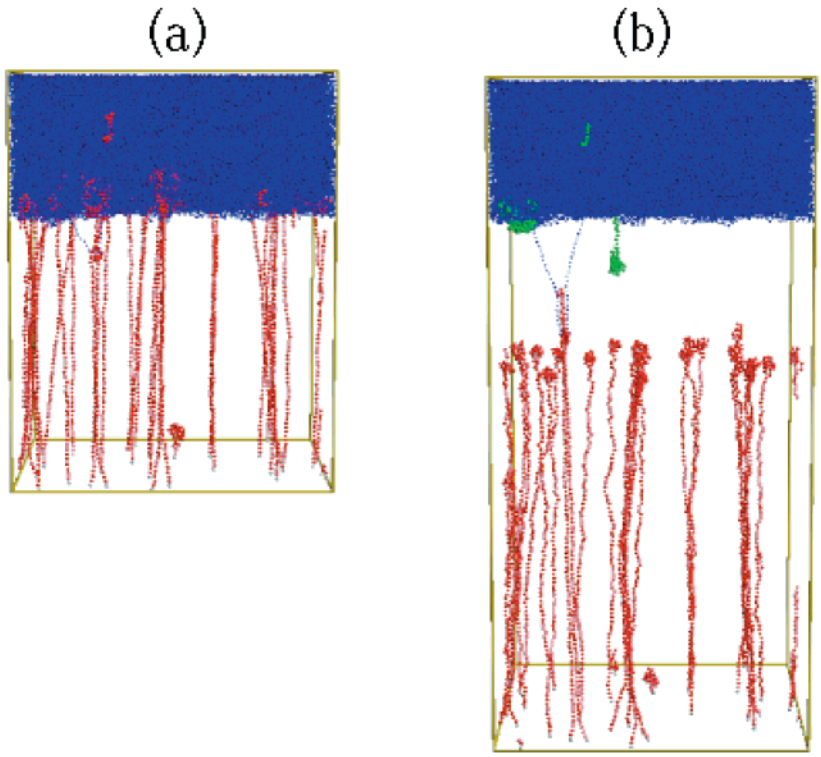

Figure 4. Chain configurations at two times during a tensile pull simulation for $N_t = 100$ with $T = 0.3\epsilon/k_B$, pull velocity $v = 0.167\sigma\tau^{-1}$, and $k_\theta = 0.0$. Elapsed times shown are (a) 300τ and (b) 600τ. The red monomers belong to tethered chains, and blue monomers belong to melt chains. Green monomers belong to sections of tethered chains that are no longer attached to the bottom substrate. Raster3D[31] is used to render the images.

well below T_g. These data have the same qualitative behavior on N_t as the data in Figure 7a; however, it is less dependent on the pulling velocity v, and the crossover to scission occurs at a tethered chain length close to N_e for both values of v. The normal mode relaxation time of a chain in an entangled polymer melt increases as the wavelength of the mode increases.[30] Therefore, as the pulling speed v becomes slower, a larger average fraction of each tethered chain is able to pull out of the melt before breaking. As T is lowered below the glass transition, however, the dynamics are dominated by the increased monomeric friction, and the velocity dependence on chain scission is considerably weaker.

This is more clearly illustrated in Figure 8, which shows the $\langle F \rangle$ dependence over 2 decades in velocity T above and below T_g. For $T < T_g$, the data are nearly independent of the pulling speed. For $T > T_g$, Figure 8 includes data for an un-cross-linked melt as well as a cross-linked network. In most applications, polymer adhesives are cross-linked when T is above T_g in order to improve mechanical properties. For large v, the data show that the amount of chain scission depends little on whether or not the polymer melt is cross-linked because the melt chains cannot relax over short times. This weak dependence of $\langle F \rangle$ on cross-linking at large v can also be seen in Figure 7a (open squares). Presumably, if v is decreased further in the un-cross-linked system for $T > T_g$, then the chains would pull out completely of the polymer liquid. However, for the cross-linked network at $T > T_g$, the value of $\langle F \rangle$ should begin to saturate for the lowest pulling velocity, albeit with less chain scission than for all the systems below T_g. Extensive simulations on entangled melts[27] have determined that the entanglement time $\tau_e \approx 1400\tau$, which is the average time needed for a chain to crossover from Rouse-like to reptation-like dynamics. The smallest values of v in Figure 8 correspond to pullout times (i.e., the time required to completely separate the pulling wall from the melt) that are 100 times larger than τ_e.

To further investigate the role of entanglements on chain dynamics, N_e is reduced by adding a finite bending energy to the chains. Figure 9a,b shows $\langle F \rangle$ vs N_t for two values of k_θ at temperatures above/below T_g. These data have the same qualitative behavior on N_t as the data in Figure 7a,b; however, the value of N_t where the onset of chain scission occurs is smaller for chains with nonzero bending interactions. This is consistent with the fact the N_e is reduced as chain stiffness is increased. The data in Figure 9a,b are from simulations using $v = 0.167\sigma\tau^{-1}$, which is the faster of the two pulling velocities seen in Figure 7. However, Figure 7b shows that for $T < T_g$ the chain scission data are nearly independent of v. Even for $T > T_g$, the effect of finite chain stiffness on N_e (and its effect on the crossover to chain scission) is clear at the higher value of v.

B. Temperature Dependence. Figure 10 shows the integrated work vs time $\mathscr{W}(t)$ as a function of T for $N_t = 100$ with $k_\theta = 0.0$. For this tethered chain length, the system is only beginning to enter the chain scission regime for all values of T. As for Figure 6, the data are shown out to sufficiently long times to show a plateau in $\mathscr{W}(t)$. The data show a steady increase in the plateau value of $\mathscr{W}(t)$ as T increases, contrary to what one might expect as T is lowered below T_g. Since almost no breaking occurs for this value of N_t, the increase in work with decreasing T can be attributed solely to an increase in the monomeric friction coefficient.

Parts a and b of Figure 11 show the integrated work vs time $\mathscr{W}(t)$ as a function of T for $N_t = 250$ with $k_\theta =$

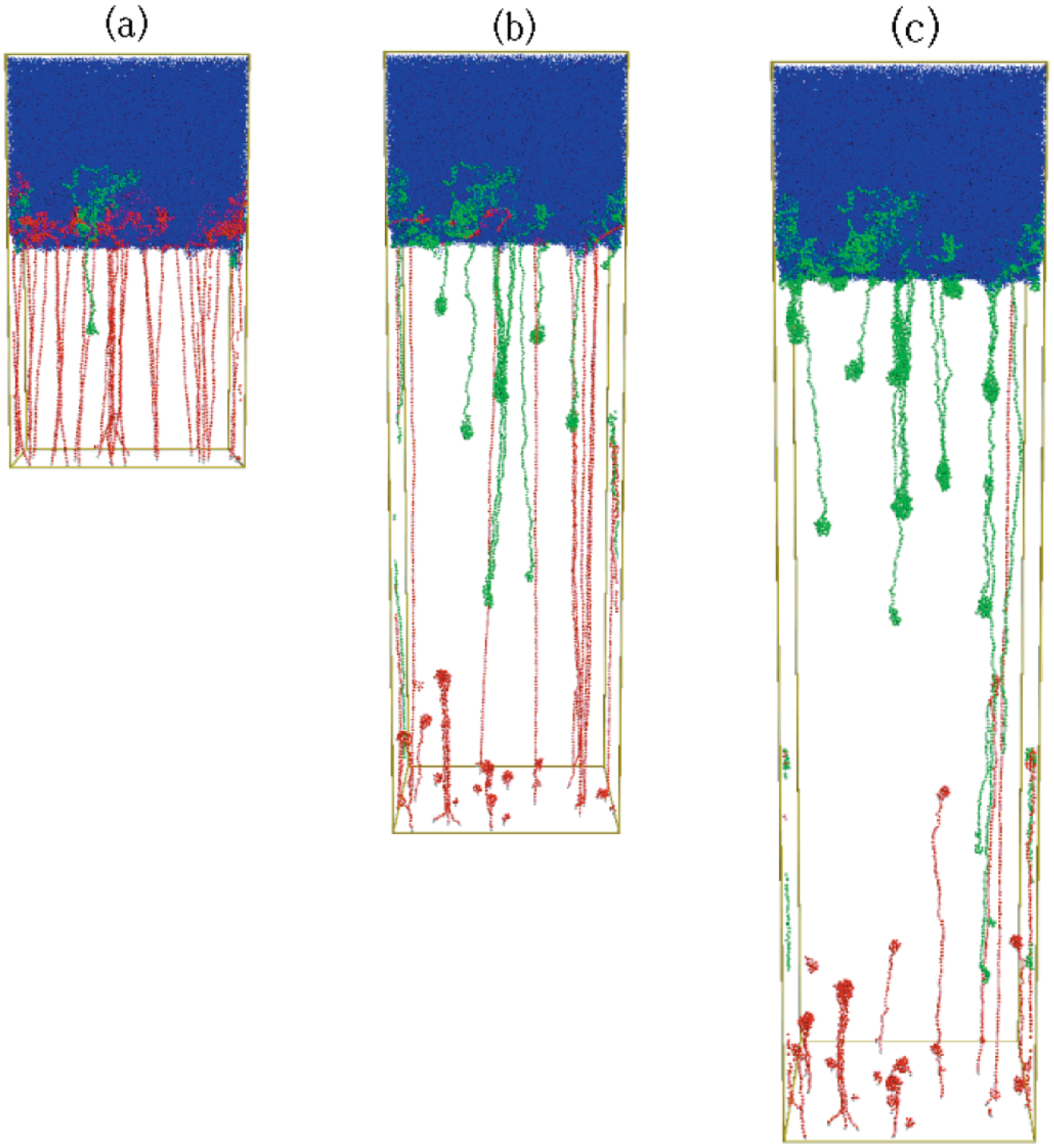

Figure 5. Chain configurations at three times during a tensile pull simulation for $N_t = 250$ with $T = 0.3\epsilon/k_B$, pull velocity $v = 0.167\sigma\tau^{-1}$, and $k_\theta = 0.0$. Elapsed times shown are (a) 300τ, (b) 900τ, and (c) 1200τ. The coloring scheme is the same as for Figure 4.

0.0 and 1.5ϵ, respectively. For $N_t = 250$, the system is well into the chain scission regime for all values of T. The work performed at early times (i.e., $t \approx 2500\tau$) increases monotonically as T decreases for both values of k_θ. However, the plateau values of $\mathscr{W}(t)$ show nonmonotonic behavior with decreasing T due to scission in the tethered chains. Chain scission occurs throughout the pull simulation, from early times $\propto \tau_e$ to times corresponding to the beginning of the $\mathscr{W}(t)$ plateau. The smaller the time necessary to allow for every tethered chain to have broken, the sooner the plateau in $\mathscr{W}(t)$ occurs. The nonmonotonic behavior, as well as the large jumps, in the plateau values for $\mathscr{W}(t)$ suggests these effects are not due to changes exclusively in the monomeric friction coefficient since this behavior is not present for tethered chains that do not break (see Figure 10). The plateau values for $T = 0.6-1.0\epsilon/k_B$ are nearly identical with a large gap between them and the higher plateau values for all $T < 0.6\epsilon/k_B$. For $k_\theta = 1.5\epsilon$, the plateau value in $\mathscr{W}(t)$ has a large jump between $T = 1.0$ and $0.6\epsilon/k_B$. However, for $T < 0.6\epsilon/k_B$, the plateau values cluster at a *lower* value of $\mathscr{W}(t)$. For $N_t > N_e$, the effects of the increasing monomeric friction with decreasing T in addition to the longer relaxation times for entangled

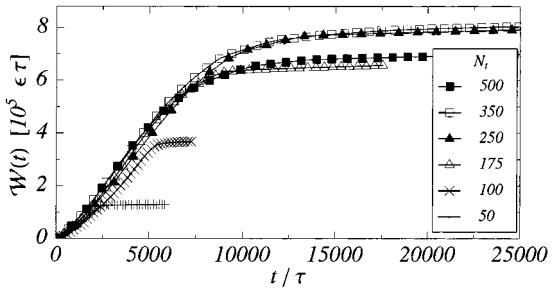

Figure 6. Total integrated work $\mathscr{W}(t)$ vs time at different tethered chain lengths N_t for $T = 0.3\epsilon/k_B$, $v = 0.0167\sigma\tau^{-1}$, and $k_\theta = 0.0$. The plateau value of $\mathscr{W}(t)$ for $N_t = 500$ is slightly lower than $N_t = 250$ and 350. This is most probably due to the proximity of the $N_t = 500$ system to the crossover between the mushroom and partially overlapped regime for the tethered chains.

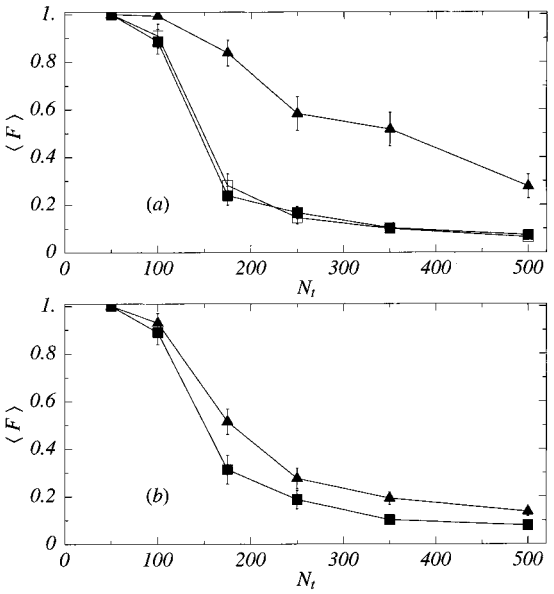

Figure 7. Average fractional length of remaining tethered chains $\langle F \rangle$ vs initial tethered chain length N_t for (a) $T = 1.0\epsilon/k_B$ and (b) $T = 0.3\epsilon/k_B$. The symbols denote $v = 0.167\sigma\tau^{-1}$ (filled square) and $v = 0.0167\sigma\tau^{-1}$ (filled triangle). The open squares show similar results for a cross-linked network with ≈18 cross-links per melt chain for $v = 0.0167\sigma\tau^{-1}$. For all data $k_\theta = 0.0$.

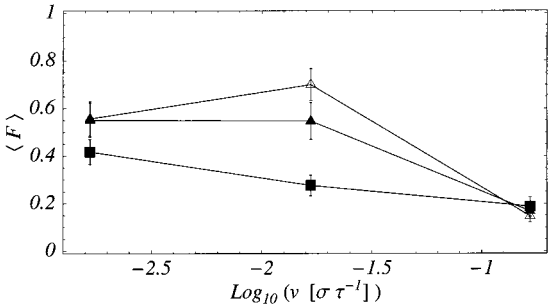

Figure 8. Average fractional length of remaining tethered chains $\langle F \rangle$ vs tensile pull velocity v for $N_t = 250$ at $T = 1.0\epsilon/k_B$ for the cross-linked (open triangles) and un-cross-linked (solid triangles) system and at $T = 0.3\epsilon/k_B$ for the un-cross-linked system (solid squares). For all data $k_\theta = 0.0$.

chains combine to produce the unexpected, nonmonotonic temperature dependence in the $\mathscr{W}(t)$ plateau values.

The temperature dependence of chain scission is shown explicitly in Figure 12, which shows $\langle F \rangle$ vs T for the systems shown in Figures 10 and 11. When $N_t =$

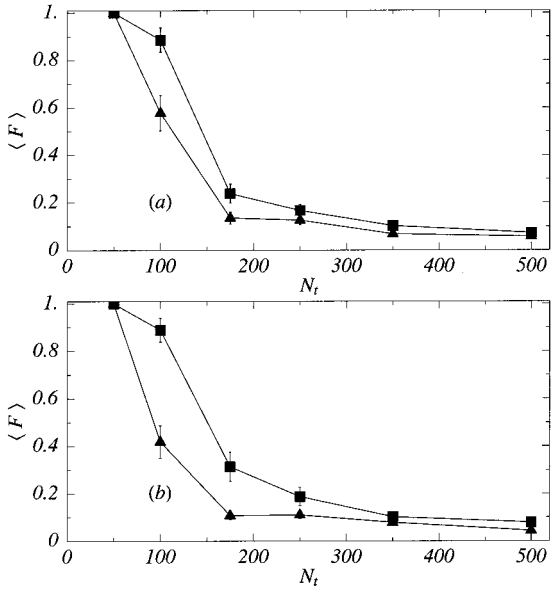

Figure 9. Average fractional length of remaining tethered chains $\langle F \rangle$ vs initial tethered chain length N_t for (a) $T = 1.0\epsilon/k_B$ and (b) $T = 0.3\epsilon/k_B$. The symbols denote $k_\theta = 0.0$ (filled square) and $k_\theta = 1.5\epsilon$ (filled triangle). For all data $v = 0.167\sigma\tau^{-1}$.

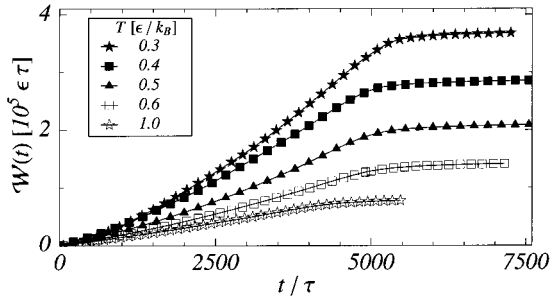

Figure 10. Total integrated work $\mathscr{W}(t)$ vs time as a function of temperature for $N_t = 100$, $v = 0.0167\sigma\tau^{-1}$, and $k_\theta = 0.0$.

100, negligible chain scission occurs for all T. For $N_t =$ 250 and $T > T_g$, the amount of chain scission is constant (within errors) for both values of k_θ. As T is lowered for $T < T_g$, $\langle F \rangle$ decreases, which helps explain the behavior $\mathscr{W}(t)$ in Figure 11. More work is done because of the increased monomeric friction at low T; however, the increase in chain scission places an upper limit on the total amount of work that can be done pulling the tethered chains before they break. For all T, chains with finite stiffness exhibit more scission than fully flexible chains, which is consistent with the data for $\langle F \rangle$ in Figure 9 which support the fact that N_e is reduced as the bending energy increases. The presence of bending stiffness for the chains in Figure 11b cannot directly account for the small drop in the plateau value of $\mathscr{W}(t)$ for $T < 0.6\epsilon/k_B$. The chains with finite stiffness should more readily mix for a given N_t and Σ; therefore, the drop in the work of adhesion cannot be attributed to phase separation of the tethered chains from the melt.

In addition to monitoring the amount of chain scission in the tethered chains, the number of broken bonds on melt chains has also been measured. For the fully flexible chains, $k_\theta = 0.0$, a large number of bonds in the melt are broken during a pull simulation for $T \geq 0.6\epsilon/k_B$. However, for $T < 0.6\epsilon/k_B$ the number of melt chain bonds that break drops suddenly to zero. For $k_\theta = 1.5\epsilon$, a large number of bonds in the melt are broken for $T = 1.0\epsilon/k_B$, the number dropping to zero for $T < 1.0\epsilon/k_B$.

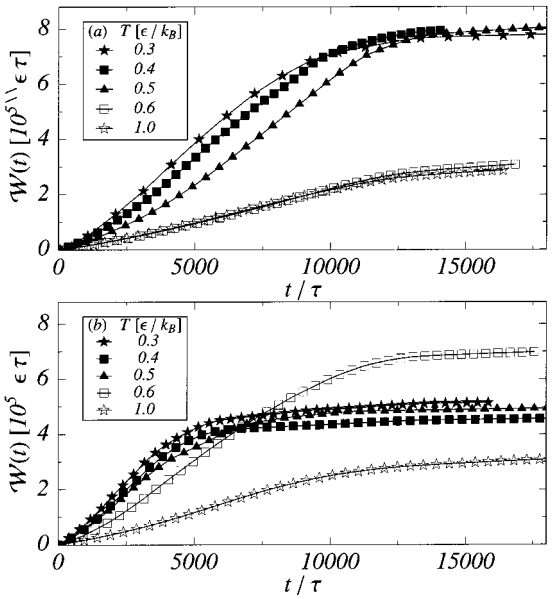

Figure 11. Total integrated work $\mathscr{W}(t)$ vs time as a function of temperature for $N_t = 250$ and $v = 0.0167\sigma\tau^{-1}$: (a) $k_\theta = 0.0$; (b) $k_\theta = 1.5\epsilon$.

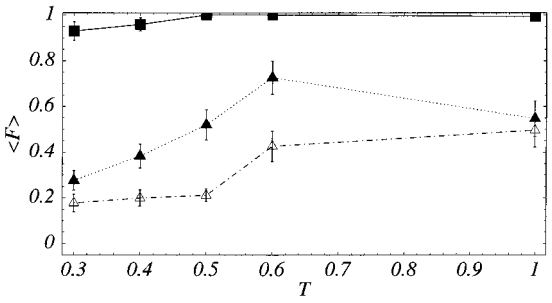

Figure 12. Average fractional length of remaining tethered chains $\langle F \rangle$ vs temperature T for $v = 0.0167\sigma\tau^{-1}$. The symbols denote $N_t = 100$, $k_\theta = 0.0$ (filled square), $N_t = 250$, $k_\theta = 0.0$ (filled triangle), and $N_t = 250$, $k_\theta = 1.5\epsilon$ (open triangle).

The explanation for this behavior is unclear; however, there seems to be a correlation in the work done and breaking in the melt chains. Specifically, the large jumps in the plateau values of $\mathscr{W}(t)$ (Figure 11a,b) occur when the number of broken melt bonds drops suddenly to zero.

IV. Conclusion

In this study we present results from the first large-scale MD simulations to study the dynamics of tethered chains in a dense polymer melt and their effects on adhesion in a 3D, realistic polymer model. Data are presented which show a crossover from pure chain pullout to chain scission which depends on the length of the tethered chains relative to the bulk entanglement length. For $T < T_g$, the length of the tethered chains near this crossover to scission is consistent with N_e (with/without bending stiffness) for the bead−spring model used in this study. This result agrees with experiments on reinforcing the interface between two immiscible, glassy polymers with block copolymers. These experiments show evidence of copolymer scission and large increases in the work of adhesion, when the molecular weight of the copolymer is comparable to the entanglement length.

However, the experimental data also suggest that in some cases the increase in the work of adhesion is due to crazing. The implication is that the copolymer block entangled in the melt transfers sufficient stress to initiate crazing. But crazing is not observed in our simulations with small values of the wall interaction energy ϵ_{wall} even for large N_t and $T < T_g$. Simulations using small values of ϵ_{wall} correspond to experiments on immiscible glassy polymers, because in both cases the attractive forces across interface are too small to initiate crazing in the absence of compatibilizers. Simulations were also performed with larger values of ϵ_{wall} to investigate the inverse problem: could the presence of crazing (due to a strong interaction between the melt and the wall) alter chain scission? These simulations showed that chain scission is virtually unaffected by the presence of crazing (i.e., voids) in the melt. The lack of crazing with small ϵ_{wall} might be because of the relatively low tethered chain areal densities simulated. Crazing could occur at small ϵ_{wall} with values of Σ larger than those in the mushroom regime but still low enough to stay out of the completely phase-separated regime (see Figure 1).

Future work will include developing algorithms to efficiently equilibrate systems with tethered chains that are partially phase separated to study the possible effects on crazing. Also, these simulations are being extended to include realistic potentials so that adhesion and crazing may be studied in real materials.

References and Notes

(1) Napper, D. H. *Polymeric Stabilization of Colloidal Dispersions;* Academic: London, 1983.
(2) Russell, W. B.; Saville, D. A.; Schowalter, W. R. *Colloidal Dispersions;* Cambridge University Press: Cambridge, 1989.
(3) Klein, J. *Annu. Rev. Mater. Sci.* **1996**, *26*, 581.
(4) Brown, H. R.; Char, K.; Deline, V. R.; Green, P. F. *Macromolecules* **1993**, *26*, 4155.
(5) Riess, G.; Jolivet, Y. Polyblends and Composites. In *ACS Advances In Chemistry Series*; Platzer, N. A. J., Ed.; American Chemical Society: Washington, DC, 1975; Vol. 142.
(6) deGennes, P. G. *Macromolecules* **1980**, *13*, 1069.
(7) Aubouy, M.; Fredrickson, G. H.; Pincus, P.; Raphaël, E. *Macromolecules* **1995**, *28*, 2979.
(8) Grest, G. S. *J. Chem. Phys.* **1996**, *105*, 5532.
(9) Léger, L.; Raphaël, E.; Hervet, H. Surface-Anchored Polymer Chains: Their Role in Adhesion and Friction. In *Advances in Polymer Science*; Granick, S., Ed.; Springer: Berlin, 1999; Vol. 138.
(10) Deruelle, M.; Léger, L.; Tirrell, M. *Macromolecules* **1995**, *28*, 7419.
(11) Creton, C.; Kramer, E. J.; Hadziioannou, G. *Macromolecules* **1991**, *24*, 1846.
(12) Washiyama, J.; Kramer, E. J.; Creton, C. F.; Hui, C.-Y. *Macromolecules* **1994**, *27*, 2019.
(13) Kramer, E. J.; Norton, L. J.; Dai, C.-A.; Sha, Y.; Hui, C.-Y. *Faraday Discuss.* **1994**, *98*, 31.
(14) Norton, L.; Smigolova, V.; Pralle, M.; Hubenko, A.; Dai, K.; Kramer, E.; Hahn, S.; Berglund, C.; DeKoven, B. *Macromolecules* **1995**, *28*, 1999.
(15) Dai, C.-A.; Kramer, E. J.; Washiyama, J.; Hui, C.-Y. *Macromolecules* **1996**, *29*, 7536.
(16) Stevens, M. J. *Macromolecules* **2001**, *34*, 1411.
(17) Stevens, M. J. *Macromolecules* **2001**, *34*, 2710.
(18) Baljon, A. R. C.; Robbins, M. O. *Macromolecules* **2001**, *34*, 4200.
(19) Gersappe, D.; Robbins, M. O. *Eur. Phys. Lett.* **1999**, *48*, 150.
(20) Pickett, G. T.; Jasnow, D.; Balazs, A. C. *Phys. Rev. Lett.* **1996**, *77*, 671.
(21) Sabouri-Ghomi, M.; Ispolatov, S.; Grant, M. *Phys. Rev. E* **1999**, *60*, 4460.
(22) Sides, S. W.; Grest, G. S.; Stevens, M. J. *Phys. Rev. E.* **2001**, *64*, 050802.
(23) Allen, M.; Tildesley, D. *Computer Simulation of Liquids;* Clarendon: Oxford, 1987.
(24) Kremer, K.; Grest, G. S. *J. Chem. Phys.* **1990**, *92*, 5057.
(25) Faller, R.; Müller-Plathe, F.; Heuer, A. *Macromolecules* **2000**, *33*, 6602.

(26) Faller, R. Influence of Chain Stiffness on Structure and Dynamics of Polymers in the Melt. Thesis, Max-Planck-Institut für Polymerforschung, Mainz, 2000.
(27) Pütz, M.; Kremer, K.; Grest, G. S. *Europhys. Lett.* **2000**, *49*, 735. The simulations in this paper used a purely repulsive interaction between nonbonded monomers and a FENE interaction between bonded monomers. The N_e for this model is expected to be very similar to that of the model used in the present study.
(28) Faller, R.; et al., unpublished results.
(29) Plimpton, S. *J. Comput. Phys.* **1995**, *117*, 1.
(30) Kremer, K.; Grest, G. S. Entanglement Effects In Polymer Melts and Networks. In *Monte Carlo and Molecular Dynamics Simulations in Polymer Science*; Binder, K., Ed.; Oxford University Press: New York, 1995.
(31) Merritt, E. A.; Bacon, D. J. *Methods Enzymol.* **1997**, *277*, 505.

MA0114739